



LAWRENCE  
LIVERMORE  
NATIONAL  
LABORATORY

LLNL-JRNL-724997

# A study of tantalum pentoxide Ta<sub>2</sub>O<sub>5</sub> structures up to 28 GPa

E. Stavrou, J. M. Zaug, S. Bastea, M. Kunz

February 22, 2017

Journal of Applied Physics.

## **Disclaimer**

---

This document was prepared as an account of work sponsored by an agency of the United States government. Neither the United States government nor Lawrence Livermore National Security, LLC, nor any of their employees makes any warranty, expressed or implied, or assumes any legal liability or responsibility for the accuracy, completeness, or usefulness of any information, apparatus, product, or process disclosed, or represents that its use would not infringe privately owned rights. Reference herein to any specific commercial product, process, or service by trade name, trademark, manufacturer, or otherwise does not necessarily constitute or imply its endorsement, recommendation, or favoring by the United States government or Lawrence Livermore National Security, LLC. The views and opinions of authors expressed herein do not necessarily state or reflect those of the United States government or Lawrence Livermore National Security, LLC, and shall not be used for advertising or product endorsement purposes.

# A study of tantalum pentoxide $Ta_2O_5$ structures up to 28 GPa

Elissaios Stavrou,<sup>1, a)</sup> Joseph M. Zaug,<sup>1, b)</sup> Sorin Bastea,<sup>1</sup> and Martin Kunz<sup>2</sup>

<sup>1)</sup>*Lawrence Livermore National Laboratory, Physical and Life Sciences Directorate, P.O. Box 808 L-350, Livermore, California 94550, USA*

<sup>2)</sup>*Advanced Light Source, Lawrence Berkeley Laboratory, Berkeley, California 94720, United States*

(Dated: 26 April 2017)

Tantalum pentoxide  $Ta_2O_5$  with the orthorhombic L- $Ta_2O_5$  structure has been experimentally studied up to 28.3 GPa (at ambient temperature) using synchrotron angle-dispersive powder x-ray diffraction (XRD). The ambient pressure phase remains stable up to 25 GPa where with increased pressure a crystalline to amorphous phase transition occurs. A detailed equation of state (EOS), including pressure dependent lattice parameters are reported. The results of this study were compared with a previous high-pressure XRD study by Li *et al.* A clear discrepancy between the ambient-pressure crystal structures and, consequently, the reported EOSs between the two studies was revealed. The origin of this discrepancy is attributed to the different crystal structures used to index the XRD patterns.

---

<sup>a)</sup>E-mail E.S. stavrou1@llnl.gov

<sup>b)</sup>E-mail J.M.Z. Zaug1@llnl.gov

## I. INTRODUCTION

Tantalum pentoxide  $Ta_2O_5$  has been extensively studied mainly due to its high refractive index, making it suitable for optical coating,<sup>1,2</sup> and its wide bandgap ( $E_g = 4$  eV) and dielectric constants, making it suitable in electronic applications such as capacitors.<sup>3</sup> Previous studies on the effect of the residual stress in the case of  $Ta_2O_5$  films suggested a strong pressure dependence of the bandgap and residual stress was shown to be the main reason for a crystalline to amorphous transition at about 18GPa.<sup>4</sup> In this context, quasi-hydrostatic pressure is widely used to mimic strain and residual stress in films of various systems. Moreover, the properties of  $Ta_2O_5$  are important for a number of practical applications, including some, *e.g.* energetic materials, that require knowledge of its high pressure equation of state (EOS). Classical energetic materials are organic molecular compounds such as 2,4,6-trinitrotoluene (TNT), Octahydro-1,3,5,7-tetranitro-1,3,5,7-tetrazocine (HMX), etc., which have a wide range of industrial and defense uses due to their stored and easily available chemical energy. An attractive way of increasing the energy density of these materials is through the addition of metallic powders, which can provide significantly more energy through oxidation. Aluminum (Al), silicon (Si), boron (B) have been widely studied in this context, and with the advent of nanopowder production technologies, many other metals are currently being considered.<sup>5,6</sup> In the nanometer domain even nominally refractory metals such as tantalum (Ta) may be amenable to explosives and propellants applications.<sup>6</sup> Ta and its oxidation have already been studied for example in thermite reactions.<sup>7</sup> Understanding and modeling the behavior and effects of metal fuels under these usage scenarios requires information on the properties of their oxides, including in particular the EOS. Experimental measurements of the structure and equation of state of  $Ta_2O_5$  at moderate pressures are however rather scarce, despite ongoing interest in its shock properties under low initial density conditions, *e.g.* powders and aerogels.<sup>8,9</sup>

The crystal structure of tantalum pentoxide at ambient conditions has been under long debate, mainly due to the difficulty to grow high quality single crystals. Nevertheless, two, so-called “low-temperature”, ambient condition crystal structures are widely accepted in the literature:<sup>10,11</sup> a) the orthorhombic  $P2mm$  (S.G. 25,  $Z=11$ , PDF-71-639,ICSD 9112)  $L\text{-}Ta_2O_5$ <sup>12</sup> and b) the orthorhombic  $Pccm$  (S.G. 49,  $Z=2$ , PDF-01-070-9177, ICSD 95462)  $\beta\text{-}Ta_2O_5$ .<sup>13</sup> Moreover, a plethora of high-temperature structures have been reported. Here,

for simplicity, we will only refer to the orthorhombic *Pmm2* (S.G. 25, Z=12, PDF-79-1375, ICSD 66366) T-Ta<sub>2</sub>O<sub>5</sub> structure synthesized by Hummel *et al.*<sup>14</sup> through high temperature chemical procedures using an intermediate TT-Ta<sub>2</sub>O<sub>5</sub> phase as a percussor. L-Ta<sub>2</sub>O<sub>5</sub> and T-Ta<sub>2</sub>O<sub>5</sub> share common structural characteristics, which are the presence of edge and corner sharing TaO<sub>6</sub> octahedra and TaO<sub>7</sub> pentagonal bipyramids.<sup>12,14,15</sup> Ta and O atoms form O-Ta-O layers in the *ab* plane and along the *c* axis. The TaO<sub>6</sub> octahedra and TaO<sub>7</sub> pentagonal bipyramids of adjacent layers are connected by corner sharing along the *c* axis, see Fig. 1. In contrast, only corner sharing TaO<sub>6</sub> octahedra are present in the  $\beta$ -Ta<sub>2</sub>O<sub>5</sub> structure,<sup>13</sup> see Fig. 1(b).

To our knowledge, only one high pressure study on bulk Ta<sub>2</sub>O<sub>5</sub> has been published, by Li *et al.*<sup>15</sup> using *in situ* synchrotron X-ray diffraction (XRD) and Raman spectroscopy. In the same study the EOS of Ta<sub>2</sub>O<sub>5</sub> up to 12 GPa, including pressure dependent lattice parameters, was reported. Moreover, a pressure induced structural transition of the starting orthorhombic phase to an amorphous form in the pressure range of 18.4 - 24.7 GPa has been observed. In their study, although the authors state that they present a high pressure study of the low-temperature orthorhombic Ta<sub>2</sub>O<sub>5</sub>, the reported cell volume and lattice parameters are in strong disagreement with those reported by Stephenson *et al.*<sup>12</sup> and Aleshina *et al.*<sup>13</sup> Instead, it seems that Li *et al.*<sup>15</sup> used the T-Ta<sub>2</sub>O<sub>5</sub> structure to index their high-pressure XRD patterns. We believe this in an important shortcoming that should be corrected, not only for the accurate knowledge of the EOS of Ta<sub>2</sub>O<sub>5</sub>, but also because future studies in other systems may be based on the results reported by Li et al. In order to resolve this issue, we have carried out a detailed synchrotron angle-dispersive powder XRD study of Ta<sub>2</sub>O<sub>5</sub> up to 28.3 GPa. We show that the XRD patterns of commercially available Ta<sub>2</sub>O<sub>5</sub> can be well indexed with the low temperature orthorhombic L-Ta<sub>2</sub>O<sub>5</sub> in agreement with Stephenson *et al.*<sup>12</sup> Moreover, we report a detailed EOS of the L-Ta<sub>2</sub>O<sub>5</sub> up to 25 GPa and a pressure induced amorphization above this pressure.

## II. METHODS

High purity and commercially available (>99.99% CERAC, INC.) Ta<sub>2</sub>O<sub>5</sub> was ground to a fine powder for x-ray diffraction (XRD) measurements. The sample including pressure sensors were loaded into diamond-anvil cell (DAC) sample chambers. Rhenium gaskets

(preindented to 40-45  $\mu\text{m}$  thick using 400  $\mu\text{m}$  diameter culets) were used to radially confine the pressurized samples. Initial sample chamber diameters were nominally 150  $\mu\text{m}$ . Ne was utilized as a pressure-transmitting medium (PTM) for XRD. Pressure was determined using a known ambient temperature EOS of gold<sup>16</sup> and also using a calibrated ruby luminescence scale.<sup>17</sup> An image plate CCD detector was used to collect pressure dependent X-ray diffraction data at the Advanced Light Source Beamline 12.2.2. An X-ray wavelength of  $\lambda = 0.4959\text{\AA}$  was selected using a Si(111) double-crystal monochromator. Exposures time varied between 10 and 30 secs. The sample to detector distance of 300 mm was determined using a CeO<sub>2</sub> (or LaB<sub>6</sub>) diffraction pattern. The X-ray beam was focused to 10 x 10  $\mu\text{m}$  using Kirkpatrick-Baez mirrors. More details on the experimental set up are given in Kunz *et al.*<sup>18</sup>

Integration of powder diffraction images to yield scattering intensity versus  $2\theta$  patterns and initial analysis were performed using the DIOPTAS<sup>19</sup> program. Calculated XRD patterns were produced using the POWDER CELL program,<sup>20</sup> for the corresponding crystal structures according to the EOSs determined experimentally in this study and also for the previously published crystalline structures all assuming continuous Debye rings of uniform intensity. Le Bail refinements were performed using the GSAS<sup>21</sup> software. Indexing of XRD patterns has been performed using the DICVOL program<sup>22</sup> as implemented in the FullProf Suite.

### III. RESULTS AND DISCUSSION

In Fig. 2(a), we plot the comparison between the experimental XRD pattern of Ta<sub>2</sub>O<sub>5</sub> with the calculated pattern of L-Ta<sub>2</sub>O<sub>5</sub> at ambient pressure. An almost perfect match, apart from a slight difference in relative intensities, is clearly observed. This is better highlighted by the Rietveld refinement given in Fig. 2(b). The cell volume and the lattice parameters obtained for Ta<sub>2</sub>O<sub>5</sub> in this study are in excellent agreement with those reported by Stephenson *et al.* for L-Ta<sub>2</sub>O<sub>5</sub>, see Table I. We present in Fig. 3 the integrated diffraction patterns of Ta<sub>2</sub>O<sub>5</sub> at selected pressures up to 28.3 GPa. The L-Ta<sub>2</sub>O<sub>5</sub> phase appears to remain stable up to 26.5 GPa followed by a pressure induced amorphization at higher pressures, see Fig. 3. With complete pressure release the amorphization is only partially lifted.

From the XRD data of Ta<sub>2</sub>O<sub>5</sub>, we determined the pressure dependent lattice parameters

TABLE I. Experimental structural parameters of L-Ta<sub>2</sub>O<sub>5</sub> and T-Ta<sub>2</sub>O<sub>5</sub> phases of Ta<sub>2</sub>O<sub>5</sub> at ambient pressure. Listed parameters include space group (SG), number of formula units in the unit cell Z, lattice parameters, cell volume, and the zero pressure bulk modulus,  $K_o$ , derived from unweighted fits to the third-order Birch-Murnaghan EOS model.

Reference	Crystal structure	SG	Z	a(Å)	b(Å)	c(Å)	$V_o$ (Å <sup>3</sup> )	$K_o$
Stephenson <i>et al.</i>	L-Ta <sub>2</sub> O <sub>5</sub>	<i>P</i> 2 $\overline{m}m$	11	6.198(5)	40.290(33)	3.888(5)	970.9	-
Hummel <i>et al.</i>	T-Ta <sub>2</sub> O <sub>5</sub>	<i>P</i> mm $\overline{2}$	12	43.996	3.894	6.209	1063.75	-
Li <i>et al.</i>	T-Ta <sub>2</sub> O <sub>5</sub>	<i>P</i> mm $\overline{2}$	12	43.997	3.894	6.209	1063.75	139
This Study	L-Ta <sub>2</sub> O <sub>5</sub>	<i>P</i> 2 $\overline{m}m$	11	6.197(6)	40.32(2)	3.813(4)	972.9(18)	199

and cell volumes, see Fig. 4. We were not able to determine the positional parameters for all atoms (*i.e.* only the positional parameters of Ta cations were refined during the Rietveld refinement), and consequently the interatomic distances, due to: a) the large difference in the Z values between Ta and O and b) the significant number ( $>100$ ) of free positional parameters. The results are compared with those published by Stephenson *et al.* shown in Figures 4. Close inspection of the compressibility of the normalized lattice parameters (Fig. 4(a)) reveals a much higher compressibility along the *c*-axis, reflecting the higher compressibility perpendicular to the layers, see Fig. 1(a)). Moreover, the axes compressibility is markedly reduced in the pressure range between  $\sim$ 16GPa (*a*-axis) and  $\sim$ 22GPa (*b* and *c*-axes). Consistent with most high-pressure EOS studies, we conducted unweighted fits ( $V_o$  is a fixed parameter) of the pressure-volume data, to a third- and second-order Birch-Murnaghan (B-M) equations of state<sup>23</sup> and determined the bulk modulus  $K_o$  and its first derivative  $K'$  (for the third-order B-M) at zero pressure for the L-Ta<sub>2</sub>O<sub>5</sub>. Although the XRD patterns of Ta<sub>2</sub>O<sub>5</sub> appear to be that of a pure crystalline phase up to 25.5 GPa, we cannot completely exclude that the gradual pressure induced amorphization starts at lower pressures. For this reason, and in order to rule out any possible effect on the reported EOS, we only included pressure-volume data up to 22 GPa in our analysis. The elastic parameters obtained this way are: a)  $K_o=199\pm2$ GPa and  $K'=0.1$  for the third-order B-M and b)  $K_o=160\pm5$ GPa for the second-order B-M. We postpone the discussion about the very low value of the  $K'$  as determined by the third-order B-M; however, we would like to note that the

results of the third-order B-M fit should be only considered as indicative of a low  $K'$ , given that its applicability range is limited to  $K' \geq 4$ .

To gain deeper insight into how  $\text{Ta}_2\text{O}_5$  responds under quasi-static compression, we conducted weighted fits and used the reduced  $\chi^2_{red}$  goodness-of-fit formalism to compare the effectiveness of three EOS models to represent the P-V data. The reduced  $\chi^2$  value closest to 1 represents the best-fit model, see Ref.<sup>24</sup> for a complete description of the procedure. The Birch-Murnaghan,<sup>23</sup> (B-M), 2<sup>nd</sup> to 4<sup>th</sup> orders, the Vinet,<sup>25</sup> and the F-f<sup>26</sup> finite strain 1<sup>st</sup> order EOS models were fit to the data, see Fig. 5. Corresponding two-dimensional confidence ellipses are plotted for the best fit model to reveal two-variable correlation information (See Figs. 6(a) and 6(b)). Bivariable confidence plots enable a more comprehensive basis for comparison of EOS parameters to alternative theoretical and/or experimental results.<sup>27</sup> Application of the F-f model to the data reveals that the pressure dependent stress, within the established errors, exhibits a linear response to applied strain (See Fig. 5(b)). There is no indication of a pressure or strain induced modification of the initial structure. The third-order B-M EOS and the first-order F-f EOS models yielded the statistically best representations of the data (See: Figure 5(a) and Table II). It is unusual that the first pressure derivative of the bulk modulus,  $K'$ , has a value near zero; within the experimental error, the pressure dependent compressibility of  $\text{Ta}_2\text{O}_5$  appears to be pressure invariant or unchanged up to approximately 25 GPa.

TABLE II. Model EOS parameters derived from fits to our  $\text{Ta}_2\text{O}_5$  data, weighted according to experimental uncertainties. Note:  $K''$  (bracketed terms) is implied for 2nd and 3rd B-M and F(f) 1<sup>st</sup> order results (See: O.L. Anderson, 1995 Oxford Univ. Press<sup>28</sup>). According to the method outlined by R.J. Angel, and with exception to the F-f EOS model,  $V_0$  is a floating parameter in EOS model fitting.<sup>27</sup>

Experimentally Weighted Fits											
B-M order	$V_0(\text{\AA}^3)$	$V_0$ esd	$K_0(\text{GPa})$	$K_0$ esd	$K'$	$K'$ esd	$K''$	$K''$ esd	$\chi^2_{red}$	Max $\Delta P$ (GPa)	KS-test
2	973.94	0.73	172.57	5.93	4.00	0.00	[-0.02]	[0.00]	4.48	3.48	0.40
3	973.57	0.55	209.07	7.91	-0.88	0.60	[-0.11]	[0.03]	1.50	2.71	0.18
4	973.22	0.45	249.05	13.78	-8.60	2.10	0.02	0.05	0.54	1.01	0.18
Vinet EOS	$V_0$	$V_0$ esd	$K_0$	$K_0$ esd	$K'$	$K'$ esd	$K''$	$K''$ esd	$\chi^2_{red}$	Max $\Delta P$	KS-test
	973.44	0.51	214.49	9.03	- 2.97	0.94	[0.00]	[0.00]	1.30	2.71	0.16
F-f order	$V_0$	$V_0$ esd	$K_0$	$K_0$ esd	$K'$	$K'$ esd	$K''$	$K''$ esd	$\chi^2_{red}$	Max $\Delta P$	KS-test
1	972.87	[1.00]	202.22	4.36	-0.25	0.35	[-0.09]	[0.01]	0.61	0.92	0.34

The low value of  $K'$  as determined by both the unweighted and the weighed fits is relatively unusual; however, low or even negative values of  $K'$  have been reported in the literature.<sup>29,30</sup> The complete elucidation of this aspect is beyond the scope of this paper as it may require single crystal diffraction in order to accurately determine interatomic distances and also thermal expansion measurements. At the present level, we can speculate on the following two explanations. One is that the L-Ta<sub>2</sub>O<sub>5</sub> crystal structure is characterized by extensive corner-sharings between TaO<sub>x</sub> polyhedra with additional open space between the polyhedra. Consequently, the compressibility is governed primarily by changes in Ta-O-Ta bond angles through rotation of multiple corner sharing polyhedra. This is in agreement with the experimentally observed higher compressibility of the  $c$  axis, see Figs. 1 and 4, the axis that is perpendicular to the O-Ta-O layers. Another way to describe the same scenario is the, almost negligible, repulsion between polyhedra as discussed in details in Ref.<sup>24</sup> A second explanation is the onset of pressure induced Bragg peak broadening, which even during the initial step of compression, signals that L-Ta<sub>2</sub>O<sub>5</sub> exhibits a tendency for disorder even at low pressures. The proposed tendency for disorder is in agreement with the results of the Raman spectroscopy measurements by Li *et al.*<sup>15</sup> This is probably, due to pressure induced frustration and/or competition between different local orderings of the Ta sublattice, as XRD intensity is, almost entirely, dominated by Ta cations. Finally, we cannot completely exclude the possibility that the extremely low  $K'$  is partially an artifact due to the pressure induced peak broadening which affects the accuracy of the p-V data.

Now we turn our attention to the disagreement between the EOS reported in our study and the one reported by Li *et al.* . Although the authors in Ref.<sup>15</sup> state that they present a high pressure study of the low temperature orthorhombic Ta<sub>2</sub>O<sub>5</sub> they used the T-Ta<sub>2</sub>O<sub>5</sub> structure for indexing their XRD patterns and further reported volumes and lattice parameters that are in agreement with those reported by Hummel *et al.*, see Table I. Given that the authors used commercially available Ta<sub>2</sub>O<sub>5</sub> powder, it is unlikely that the starting material is the T-Ta<sub>2</sub>O<sub>5</sub> allotrope, which is normally synthesized under specific chemical and temperature conditions. As clearly observed in Fig. 2(a), the calculated XRD patterns of L-Ta<sub>2</sub>O<sub>5</sub> and T-Ta<sub>2</sub>O<sub>5</sub> are hardly distinguishable based only on the positions and the relative intensities of the main Bragg peaks. This can be attributed to the common structural characteristics of these two allotropes,<sup>12,14</sup> see discussion in the introduction and Table I. However, a closer inspection of the lower intensity Bragg peaks, especially at low  $2\theta$ , can

provide a way to distinguish between the XRD patterns of these structural modifications, see inset in Fig.2(a). Unfortunately, a refinement of the experimental patterns was not provided by the authors and moreover, the low angle region of the  $2\theta$  range ( $<8^\circ$  in Ref. 1 and  $<6.4^\circ$  in Fig. 2(a)) is missing. Nevertheless, we believe that the measured XRD pattern by Li *et al.* can be more optimally indexed with the L-Ta<sub>2</sub>O<sub>5</sub> structure. From the above discussion, we conclude that Li and coworkers made an unintentional error by indexing their experimental patterns with the T-Ta<sub>2</sub>O<sub>5</sub> structure and thus, reported an EOS that doesn't correspond to any crystal form of Ta<sub>2</sub>O<sub>5</sub>. Finally, it is plausible to assume that the higher critical pressure for amorphization in this study (26.5 GPa vs  $\sim$ 21 GPa in Ref.<sup>15</sup>) can be attributed to the use of neon as a PTM in this study compared to the significantly less hydrostatic (above 10 GPa) methanol-ethanol mixture<sup>31,32</sup> used by Li *et al.*

#### IV. CONCLUSION

To summarize, the high-pressure structural of Ta<sub>2</sub>O<sub>5</sub> has been explored experimentally up to 28.3 GPa using synchrotron x-ray diffraction. We have shown that the ambient phase can be more appropriately indexed with the “low-temperature” L-Ta<sub>2</sub>O<sub>5</sub> structure. The L-Ta<sub>2</sub>O<sub>5</sub> phase remains stable up to 25 GPa where pressure induced amorphization takes place. The respective bulk moduli and corresponding pressure derivatives were derived from weighted and unweighted fits using selected (relatively optimal) EOS models. We have shown that Li and co-workers have unintentionally reported an erroneous high-pressure EOS for the low temperature phase of Ta<sub>2</sub>O<sub>5</sub> based on the T-Ta<sub>2</sub>O<sub>5</sub> phase.

#### ACKNOWLEDGMENTS

E. S. thanks K. Syassen for fruitful discussions and for a critical reading of the manuscript. This work was performed under the auspices of the U. S. Department of Energy by Lawrence Livermore National Security, LLC under Contract DE-AC52-07NA27344. We thank the Joint Munitions Program (JMP - TCG-III) for supporting this study and also the high explosives science campaign II research program at Lawrence Livermore National Laboratory. The Advanced Light Source is supported by the Director, Office of Science, Office of Basic Energy Sciences, of the U.S. Department of Energy under Contract No. DE-AC02-

## REFERENCES

<sup>1</sup>M. H. Asghar, F. Placido, and S. Naseem, *J. Phys. D: Appl. Phys.* **40**, 2065 (2007).

<sup>2</sup>T. Damart, E. Coillet, A. Tanguy, and D. Rodney, *J. Appl. Phys.* **119**, 175106 (2016).

<sup>3</sup>J. D. Prymak, in *Conference Record of 1998 IEEE Industry Applications Conference. Thirty-Third IAS Annual Meeting (Cat. No.98CH36242)*, Vol. 2 (1998) pp. 1129–1137 vol.2.

<sup>4</sup>S. Dhawan, T. Dhawan, and A. G. Vedeshwar, *J. Alloys Compd.* **657**, 366 (2016).

<sup>5</sup>E. L. Dreizin, *Prog. Energy Combust. Sci.* **35**, 141 (2009).

<sup>6</sup>C. W. Won, H. H. Nersisyan, H. I. Won, and J. H. Lee, *Curr. Opin. Solid State Mater. Sci.* **14**, 53 (2010).

<sup>7</sup>O. G. Cervantes, J. D. Kuntz, A. E. Gash, and Z. A. Munir, *Combust. Flame* **158**, 117 (2011).

<sup>8</sup>J. E. Miller, T. R. Boehly, D. A. Meyerhofer, and J. H. Eggert, in *Shock compression of condensed matter - 2007, pts 1 and 2*, AIP Conference Proceedings, Vol. 955, edited by M. Elert, M. Furnish, R. Chau, N. Holmes, and J. Nguyen (2007) pp. 71–74, Conference of the American-Physical-Society-Topical-Group on Shock Compression of Condensed Matter, Waikoloa, HI, JUN 24-29, 2007.

<sup>9</sup>G. Fenton, D. Grady, and T. Vogler, in *Shock compression of condensed matter - 2011, pts 1 and 2*, AIP Conference Proceedings, Vol. 1426, edited by M. Elert, W. Buttler, J. Borg, J. Jordan, and T. Vogler (2012) 7th Biennial Conference of the American-Physical-Society-Topical-Group on Shock Compression of Condensed Matter, Chicago, IL, JUN 26-JUL 01, 2011.

<sup>10</sup>J.-Y. Kim, B. Magyari-Koepe, K.-J. Lee, H.-S. Kim, S.-H. Lee, and Y. Nishi, *Phys. Status Solidi Rapid Res. Lett.* **8**, 560 (2014).

<sup>11</sup>S. Perez-Walton, C. Valencia-Balvin, A. C. M. Padilha, G. M. Dalpian, and J. M. Osorio-Guillen, *J. Phys.: Condens. Matter* **28** (2016).

<sup>12</sup>N. Stephenson and R. Roth, *Acta Crystallogr. Sect. B* **27**, 1037 (1971).

<sup>13</sup>L. Aleshina and S. Loginova, *Crystallogr. Rep.* **47**, 415 (2002).

<sup>14</sup>H.-U. Hummel, R. Fackler, and P. Remmert, *Chemische Berichte* **125**, 551 (1992).

<sup>15</sup>Q. Li, H. Zhang, B. Cheng, R. Liu, B. Liu, J. Liu, Z. Chen, B. Zou, T. Cui, and B. Liu, *J. Appl. Phys.* **115**, 193512 (2014).

<sup>16</sup>M. Matsui, International Conference On High Pressure Science and Technology, Joint AIRAPT-22 and HPCJ-50 **215**, 012197 (2010).

<sup>17</sup>K. Syassen, *High Pres. Res.* **28**, 75 (2008).

<sup>18</sup>M. Kunz, A. MacDowell, W. Caldwell, D. Cambie, R. Celestre, E. Domning, R. Duarte, A. Gleason, J. Glossinger, N. Kelez, D. Plate, T. Yu, J. Zaug, H. Padmore, R. Jeanloz, A. Alivisatos, and S. Clark, *J. Synchrotron Radiat.* **12**, 650 (2005).

<sup>19</sup>C. Prescher and V. B. Prakapenka, *High Pres. Res.* **35**, 223 (2015).

<sup>20</sup>W. Kraus and G. Nolze, *J. Appl. Crystallogr.* **29**, 301 (1996).

<sup>21</sup>A. C. Larson and R. B. V. Dreele, “GSAS: General structure analysis system report LAUR 86-748,” Tech. Rep. (Los Alamos National Laboratory, 2000).

<sup>22</sup>A. Boultif and D. Louër, *J. Appl. Crystallogr.* **37**, 724 (2004).

<sup>23</sup>F. Birch, *J. Geophys. Res.* **83**, 1257 (1978).

<sup>24</sup>E. Stavrou, M. R. Mana, J. M. Zaug, I.-F. W. Kuo, P. F. Pagoria, B. Kalkan, J. C. Crowhurst, and M. R. Armstrong, *J. Chem. Phys.* **143**, 144506 (2015).

<sup>25</sup>P. Vinet, J. Ferrante, J. R. Smith, and J. H. Rose, *J. Phys. C* **19**, L467 (1986).

<sup>26</sup>F. Birch, *Phys. Rev.* **71**, 809 (1947).

<sup>27</sup>R. J. Angel, *Rev. Mineral Geochem.* **41**, 35 (2000).

<sup>28</sup>O. Anderson, *Equations of State of Solids in Geophysics and Ceramic Science* (Oxford University Press Inc, 1995).

<sup>29</sup>I. Efthimiopoulos, T. Lochbiler, V. Tsurkan, A. Loidl, V. Felea, and Y. Wang, *J. Phys. Chem. C* **121**, 769 (2017).

<sup>30</sup>H. Fang and M. T. Dove, *Phys. Rev. B* **87**, 214109 (2013).

<sup>31</sup>S. Klotz, J.-C. Chervin, P. Munsch, and G. L. Marchand, *J. Phys. D: Appl. Phys.* **42**, 075413 (2009).

<sup>32</sup>R. J. Angel, M. Bujak, J. Zhao, G. D. Gatta, and S. D. Jacobsen, *J. Appl. Crystallogr.* **40**, 26 (2007).

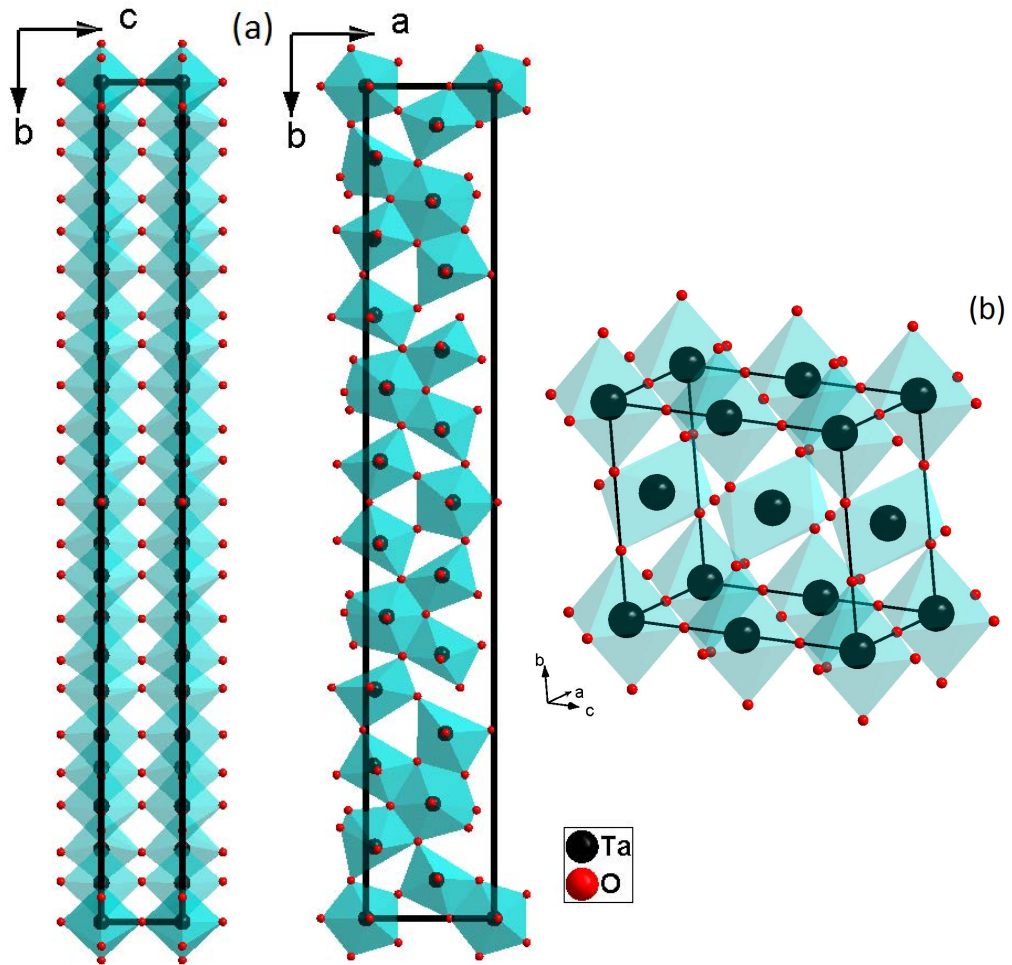


FIG. 1. Schematic representations of: a) the L-Ta<sub>2</sub>O<sub>5</sub> structure along the *a* (left) and *c* (right) axis and b) the  $\beta$ -Ta<sub>2</sub>O<sub>5</sub>.

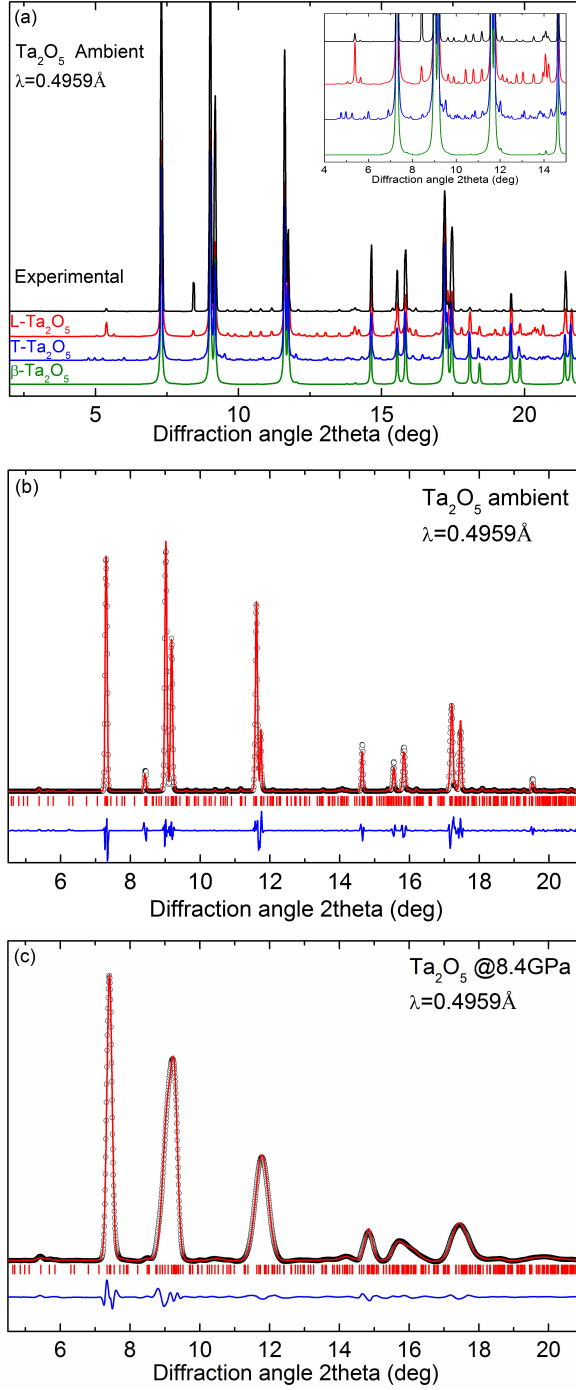


FIG. 2. (a) Calculated XRD patterns of  $\text{L-Ta}_2\text{O}_5$ ,  $\beta\text{-Ta}_2\text{O}_5$  and  $\text{T-Ta}_2\text{O}_5$  at ambient pressure. The experimental XRD pattern of this study is also shown. (b) Rietveld refinement results for  $\text{Ta}_2\text{O}_5$  at ambient pressure and (c) at 8.4 GPa,  $\text{L-Ta}_2\text{O}_5$  structure. Symbols correspond to the measured profile, the red solid lines represent the results of Rietveld refinements. The difference curve (blue curve) is also plotted. Vertical tick marks indicate Bragg peak positions.

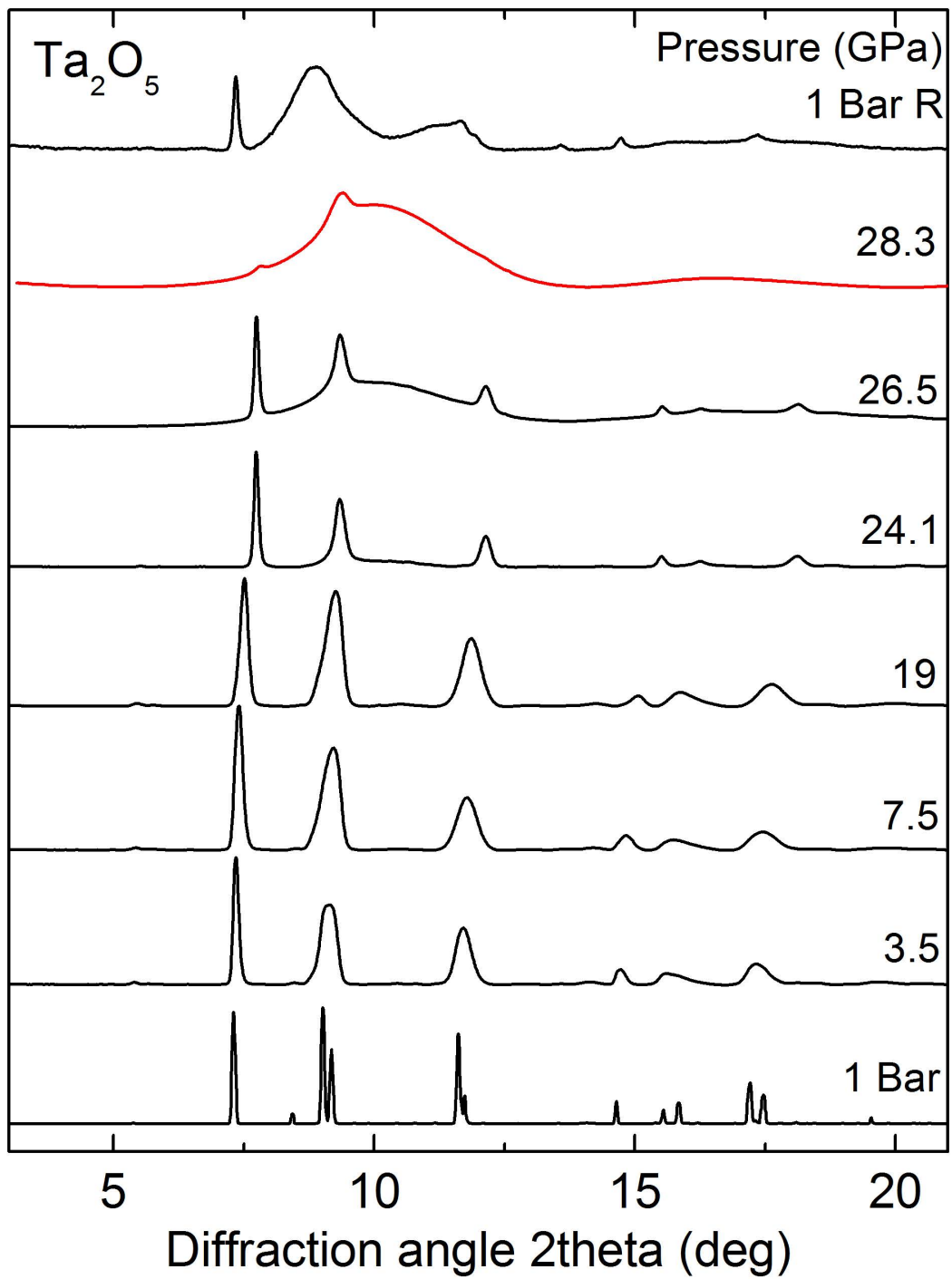


FIG. 3. XRD patterns of  $\text{Ta}_2\text{O}_5$  at selected pressures.

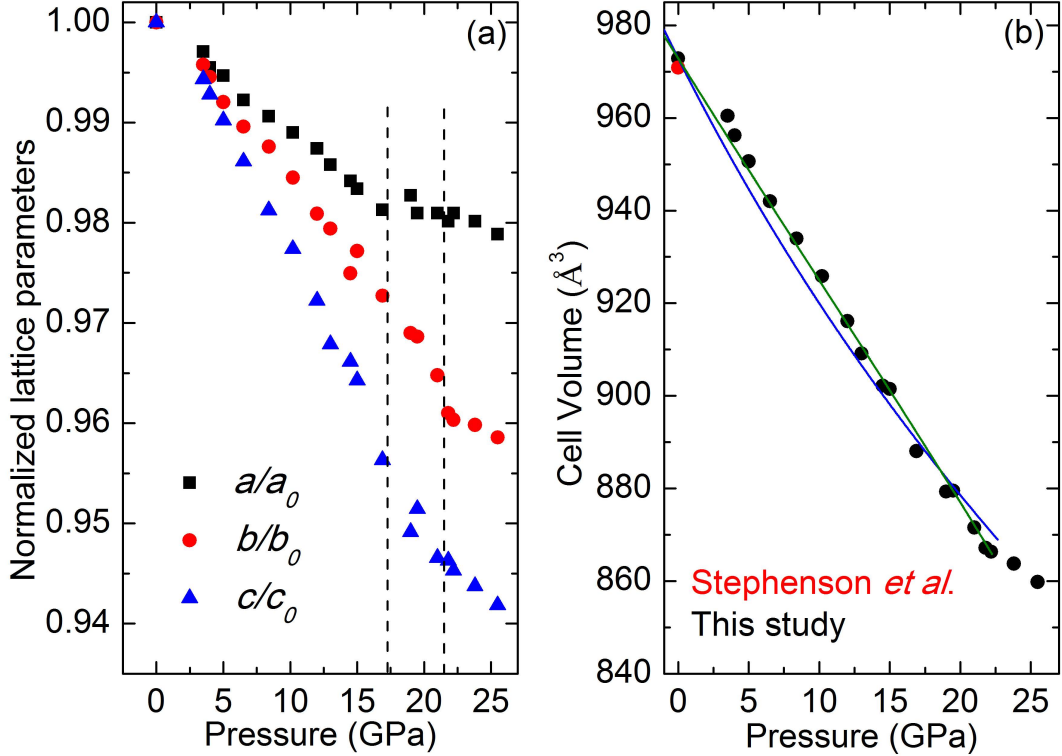


FIG. 4. (a) Pressure dependence of the normalized lattice parameters and (b) pressure-volume data for the L-Ta<sub>2</sub>O<sub>5</sub>. The solid green and blue lines are third- and second-order B-M equation of state unweighted fits respectively, of the L-Ta<sub>2</sub>O<sub>5</sub> phase experimental data; Vo was a fixed fitting parameter. The vertical dashed lines in (a) mark the pressure range of the observed decrease of the axes compressibility, see text for details.

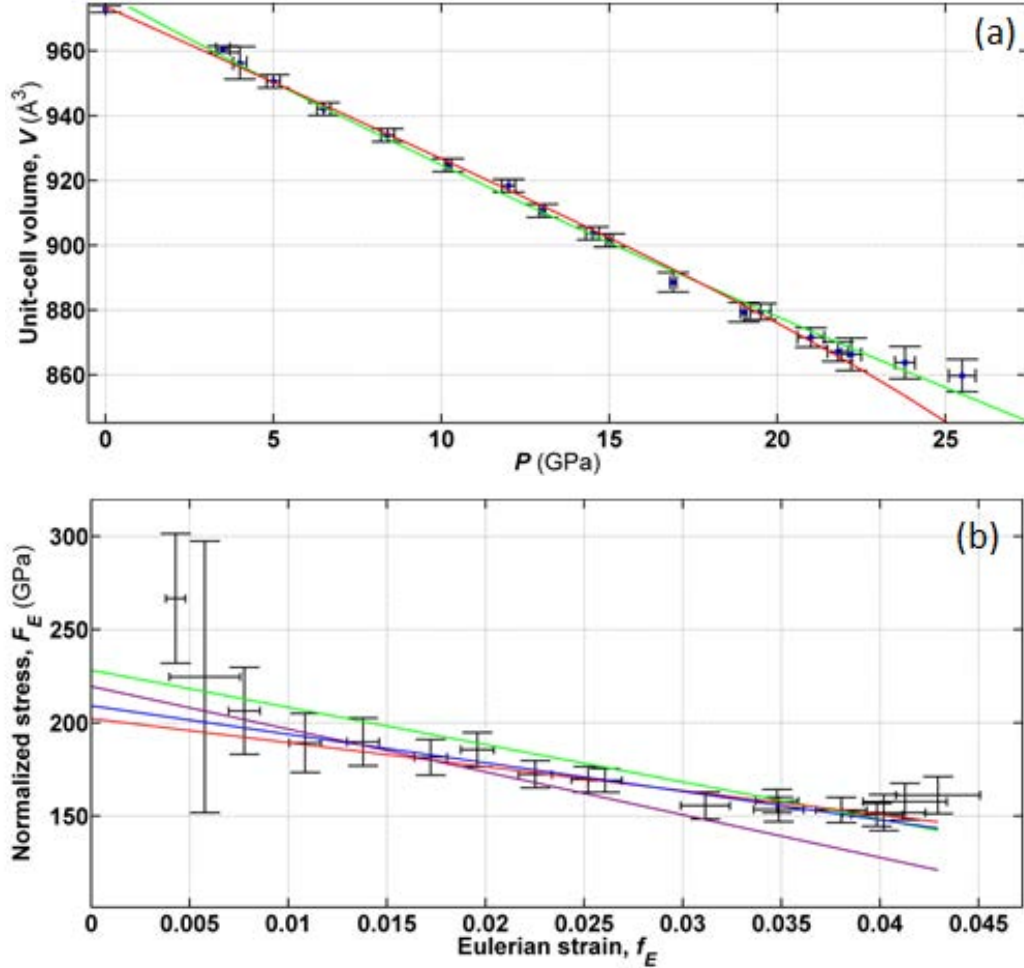


FIG. 5. (a) Third order Birch-Murnaghan EOS model weighted fit to Ta<sub>2</sub>O<sub>5</sub> data. The red line represents a weighted fit and the green line is from an unweighted fit. b) First-order F-f EOS model weighted fit to Ta<sub>2</sub>O<sub>5</sub> data. The red line represents a weighted fit and the green line is from an unweighted fit. The violet line represents a weighted Vinet EOS fit and the blue line is from a third-order B-M EOS model fit to the data.

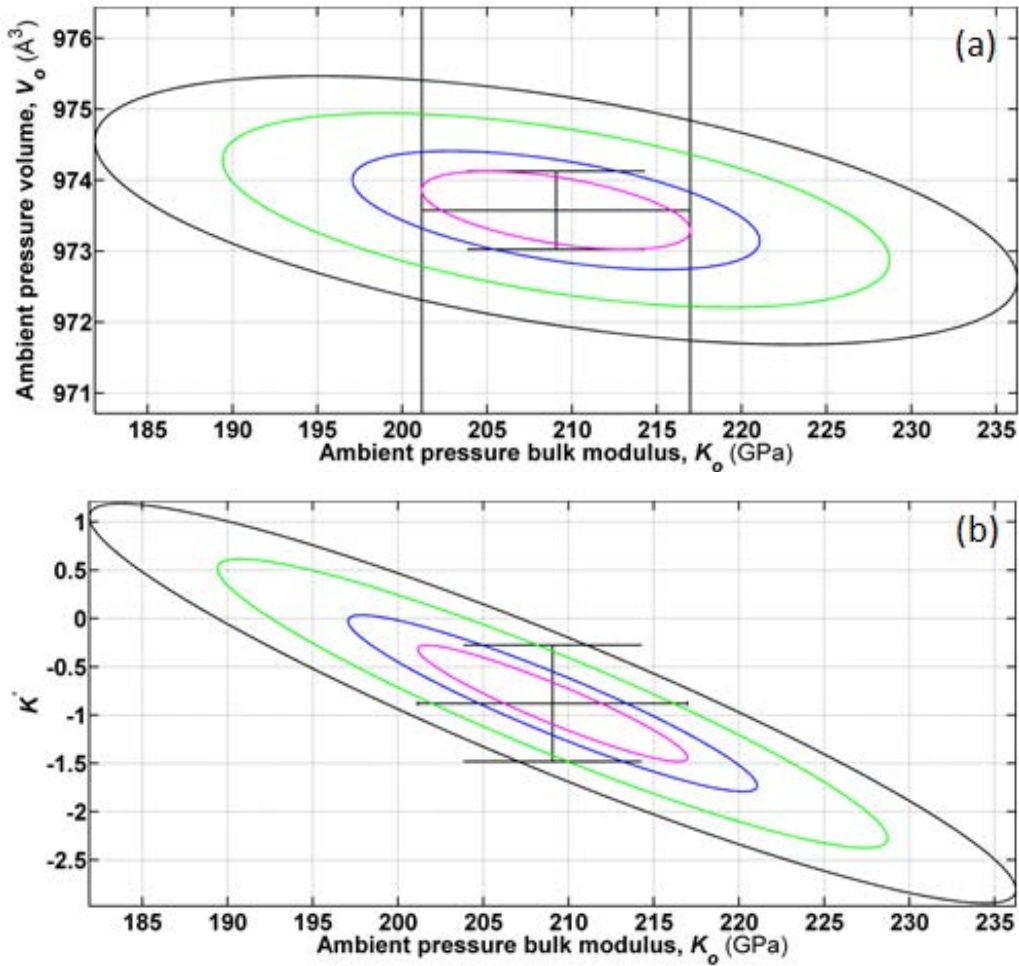


FIG. 6. Confidence ellipses from a third order Birch-Murnaghan EOS model weighted fit to Ta<sub>2</sub>O<sub>5</sub> data. (a)  $V_o$  vs.  $K_o$ , and b)  $K'$  vs.  $K_o$ . The magenta colored ellipse is 0.607- $\sigma$  (50.3% confidence), blue is 1- $\sigma$  (68.3% confidence), green is 2- $\sigma$  (95.4% confidence), and the black ellipse is 3- $\sigma$  (99.7% confidence).